AGU PUBLICATIONS

Geophysical Research Letters

RESEARCH LETTER
10.1002/2015GL066624

Key Points:
- Observations of sea surface height using spaceborne GPS-Reflectometry are shown for the first time
- Sea surface height is estimated using GPS-Reflectometry data from the TechDemoSat-1 satellite
- Sea surface height estimates from TechDemoSat-1 agree well with DTU10 mean sea surface

Correspondence to:
M. P. Clarizia,
clarizia@umich.edu

Citation:
Clarizia, M. P., C. Ruf, P. Cipollini, and C. Zuffada (2016), First spaceborne observation of sea surface height using GPS-Reflectometry, *Geophys. Res. Lett.*, *43*, 767–774, doi:10.1002/2015GL066624.

Received 16 OCT 2015
Accepted 2 JAN 2016
Accepted article online 6 JAN 2016
Published online 26 JAN 2016
Corrected 15 MAR 2016

This article was corrected on 15 MAR 2016. See the end of the full text for the details.

First spaceborne observation of sea surface height using GPS-Reflectometry

Maria Paola Clarizia[1], Christopher Ruf[1], Paolo Cipollini[2], and Cinzia Zuffada[3]

[1]Climate and Space Sciences and Engineering, University of Michigan, Ann Arbor, Michigan, USA, [2]National Oceanography Centre, Southampton, UK, [3]Jet Propulsion Laboratory, California Institute of Technology, Pasadena, California, USA

Abstract An analysis of spaceborne Global Positioning System reflectometry (GPS-R) data from the TechDemoSat-1 (TDS-1) satellite is carried out to image the ocean sea surface height (SSH). An SSH estimation algorithm is applied to GPS-R delay waveforms over two regions in the South Atlantic and the North Pacific. Estimates made from TDS-1 overpasses during a 6 month period are aggregated to produce SSH maps of the two regions. The maps generally agree with the global DTU10 mean sea surface height. The GPS-R instrument is designed to make bistatic measurements of radar cross section for ocean wind observations, and its altimetric performance is not optimized. The differences observed between measured and DTU10 SSH can be attributed to limitations with the GPS-R instrument and the lack of precision orbit determination by the TDS-1 platform. These results represent the first observations of SSH by a spaceborne GPS-R instrument.

1. Introduction

Global Navigation Satellite System reflectometry (GNSS-R) uses reflections by the surface of the Earth of the signal transmitted by navigation satellites to infer a number of geophysical parameters [*Gleason and Gebre-Egziabher*, 2009]. The technique was first proposed by *Hall and Cordey* [1988], and over the years it has proved particularly effective for sensing oceanic parameters, such as wind speed [*Garrison et al.*, 2002; *Katzberg et al.*, 2006; *Gleason*, 2013; *Clarizia et al.*, 2014; *Foti et al.*, 2015] and sea surface height or SSH [*Lowe et al.*, 2002; *Hajj and Zuffada*, 2003; *Rius et al.*, 2010; *Cardellach et al.*, 2013]. The successful demonstration of spaceborne GNSS-R for ocean wind speed retrieval, shown in *Gleason et al.* [2013], *Clarizia et al.* [2014], and *Foti et al.* [2015], has recently led to the selection of the NASA Cyclone Global Navigation Satellite System (CYGNSS) mission [*Ruf et al.*, 2015] which will be launched in 2016 and will measure ocean surface wind speed in tropical cyclone conditions using GNSS-R payloads on a constellation of eight microsatellites. The altimetric application of GNSS-R presents different challenges from the scatterometric one since it requires an accurate measurement of signal propagation time to estimate SSH, as opposed to an accurate measurement of scattered power in the case of wind speed. The use of GNSS-R for ocean altimetry was first suggested by *Martin-Neira* [1993]. Recent enhancements have been proposed, which include the use of wider bandwidth navigation signals [*Pascual et al.*, 2013] and the use of more sophisticated techniques (such as interferometric processing) to process the received waveforms [*Cardellach et al.*, 2013; *Lowe et al.*, 2014; *D'Addio et al.*, 2014].

The nominal predicted precision for SSH estimates from an individual 1 s GNSS-R measurement is 5 m [*Cardellach et al.*, 2013], but if all the aforementioned enhancements were available and applied, the precision would improve to a few tens of centimeters [see, e.g., *Martin-Neira et al.*, 2011; *Cardellach et al.*, 2013; *Camps et al.*, 2014]. Combined with the potential for very dense time and space sampling attainable from a constellation of small, low-power, and low-cost satellites, this raises the possibility of resolving small spatial and temporal scale physical processes. Measurement of SSH is the main objective of the GNSS-Reflectometry experiment on board the International Space Station, a European Space Agency experiment currently in phase A and scheduled for launch in 2019 [*Wickert et al.*, 2014].

The analysis presented here focuses on SSH estimation using data from the GNSS-R experiment on board the TDS-1 satellite [*Jales and Unwin*, 2015a]. TDS-1 was launched in July 2014, and it orbits at an altitude of 635 km, with an inclination of 98° and a 9:00 P.M. local time of ascending node. The spaceborne GNSS-R payload consists of a zenith-pointing antenna for direct GPS signal acquisition and the determination of specular point locations on the ground, a nadir-pointing antenna with a peak gain of 13.3 dBi, for capturing the GPS reflection, and a remote sensing receiver, called SGR-ReSI. The SGR-ReSI operates for 2 days out of an 8 day cycle, and generates delay Doppler maps (DDMs) of reflections from L1 GPS (1575.42 MHz) only; hence,

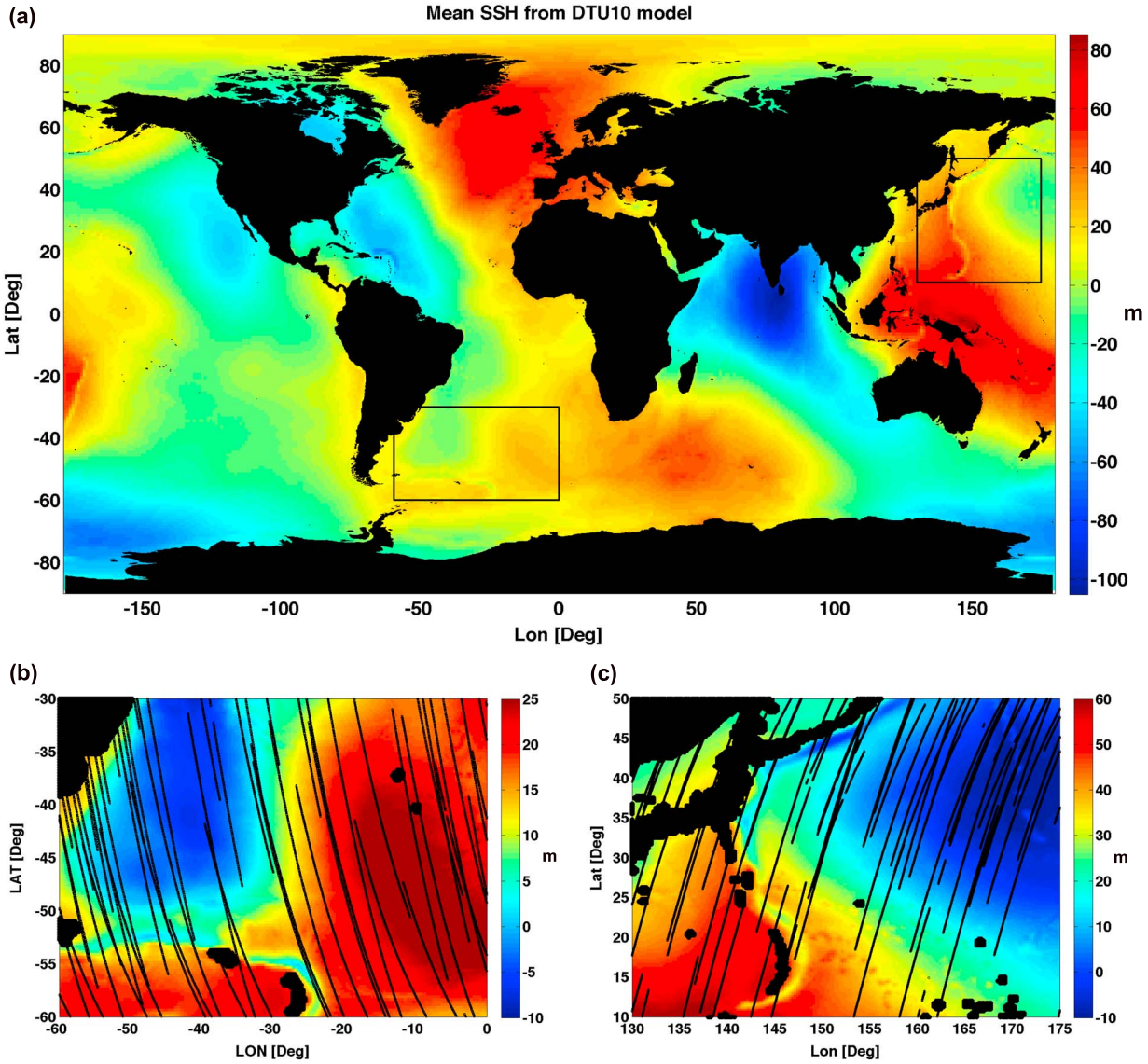

Figure 1. (a) Global map of MSSH from the DTU10 model, with test areas highlighted as black boxes. (b) Zoomed version of the MSSH for the South Atlantic region; (c) zoomed version of the MSSH for the North Pacific region. The black areas in Figures 1b and 1c represent a landmask which accounts for land plus a 50 km coastal strip. TDS-1 specular point tracks are overlaid in Figures 1b and 1c, after the quality control (QC) filter is applied.

the focus of TDS-1 is on GPS-Reflectometry (GPS-R). Since March 2015 a large data set of DDMs collected over ocean, land, and sea has been made available to the public on a dedicated website (www.merrbys.co.uk). The data set spans a 6 month time period from September 2014 to February 2015 and is provided in the form of 1 s DDMs plus the corresponding metadata. The geographical distribution of the acquisitions is quite uniform over the oceans [see *Foti et al.*, 2015] and comprises more than 1 million DDMs.

In this study, the feasibility of SSH estimation from spaceborne altitudes using GPS-R is demonstrated for the first time, using TDS-1 data. We select two test regions over the ocean and retrieve SSH from TDS-1 tracks of GPS reflections. The results show reasonable agreement with a ground truth mean sea surface height (MSSH) map developed at the Danish Technical University and known as DTU10 [*Andersen*, 2010; *Andersen et al.*, 2010]. The data set used for this study is described in section 2. Section 3 describes the SSH estimation algorithm. Section 4 shows the results and comparison of the SSH obtained from TDS-1 with the ground truth. Section 5 draws the conclusions and discusses some possible future work.

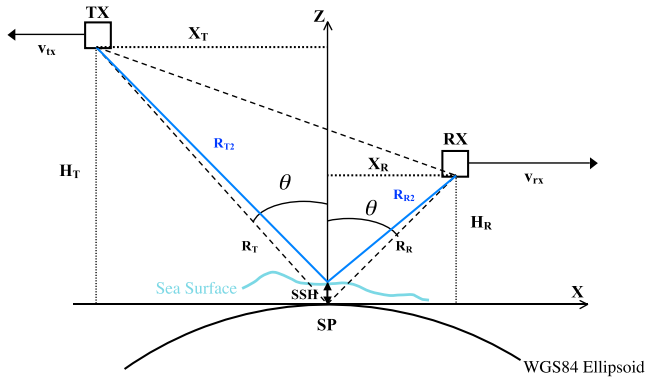

Figure 2. SSH measurement geometry. The time delays τ_2 and τ_1 are represented, respectively, by the blue reflected minus direct path and the black reflected minus direct path. The geometry assumes that the transmitter (TX), specular point (SP), and receiver (RX) are in the *x-z* plane.

2. Description of GPS-R Data

The data set used in this study consists of onboard-generated DDMs of GPS scattered power from the ocean surface [*Gleason*, 2013], made of 128 delay pixels by 20 Doppler pixels, with a Doppler resolution of 500 Hz and a delay resolution of 0.25 chips [*Jales and Unwin*, 2015a, 2015b], where 1 chip is approximately 1 μs. The 0.25 chip delay resolution corresponds to 75 m in along-range distance, which maps to SSH variations of between ~37 m and ~50 m, depending on the measurement geometry [see *Cardellach et al*., 2013, equation (12)]. The accompanying metadata include information about the receiving antenna gain at the specular point, the geometry of the measurement, including the GPS transmitter and TDS-1 receiver positions, and the predicted position of the specular point on the Earth surface [*Jales and Unwin*, 2015b].

For our altimetric analysis, we select two test regions of the ocean characterized by relatively large variations in MSSH. The regions are in the South Atlantic and North Pacific (see Figure 1a). Also shown in Figure 1a is the global DTU10 MSSH, which is used as ground truth in this study. This is the sum of the geoid and mean dynamic topography of the ocean and is available in gridded format with a 1/60° resolution in latitude and longitude. The DTU10 MSSH for the two test regions is also illustrated in Figures 1b and 1c. Also shown are the locations of the TDS-1 SSH samples used in this study. The −106 m to +87 m variations in MSSH shown in Figure 1 are mostly due to the spatial variations in the geoid.

The asynchronous nature of the TDS-1 and GPS satellite orbits, which results in the specular points not repeating at the same locations or with a recurring revisit time, combined with the fact that the GPS-R payload on TDS-1 is only switched on for a few hours every 8 days, makes the available data quite sparse in space and time. Therefore, we aggregate all available samples over the 6 month period for the two test regions. It is for this reason that we use the MSSH as ground truth, since it represents gross features of the SSH variations over large spatial and temporal scale sizes and neglects the shorter scale sea level anomaly changes.

A landmask is applied, which filters out the samples over land and over a coastal strip 50 km wide. The peak gain of the receiving antenna is lower than the ~20 dBi recommended for high-quality spaceborne altimetry [*Martin-Neira et al*., 2011; *Cardellach et al*., 2013; *Zuffada et al*., 2015]. The antenna has also a fixed (not beam-steered) pattern that rolls off in gain away from its peak, so a range of antenna gains needs to be used to provide sufficient samples. We filter the data and use all samples with antenna gain above 5 dBi. This is a lower threshold than recommended by previous investigators, and, as such, the error in the SSH estimates is higher (see section 4). The lower threshold was dictated by a desire to retain enough TDS samples to capture the structure of the SSH spatial distribution. In addition, we use only ascending orbit tracks acquired during the local night time. This removes orbital errors observed in the descending (daytime) track data and also minimizes the effects of fluctuating tropospheric and ionospheric propagation delay. The antenna gains lower bound, and the overnight sample selection represents a quality control (QC) filter, after which 55 and 59 DDM tracks are retained for the South Atlantic and the North Pacific, respectively. The tracks, overlaid on the MSSH, are shown in Figures 1b and 1c.

3. Sea Surface Height Retrieval

Our SSH estimation algorithm is based on the leading edge derivative (LED) approach described in *Hajj and Zuffada* [2003]. The algorithm is applied to the delay waveforms, which are obtained by selecting from each interpolated DDM the delay-varying scattered power at zero Doppler frequency (i.e., the central column of the DDM). To improve SSH resolution, the waveform sampling in delay is increased through interpolation, prior to

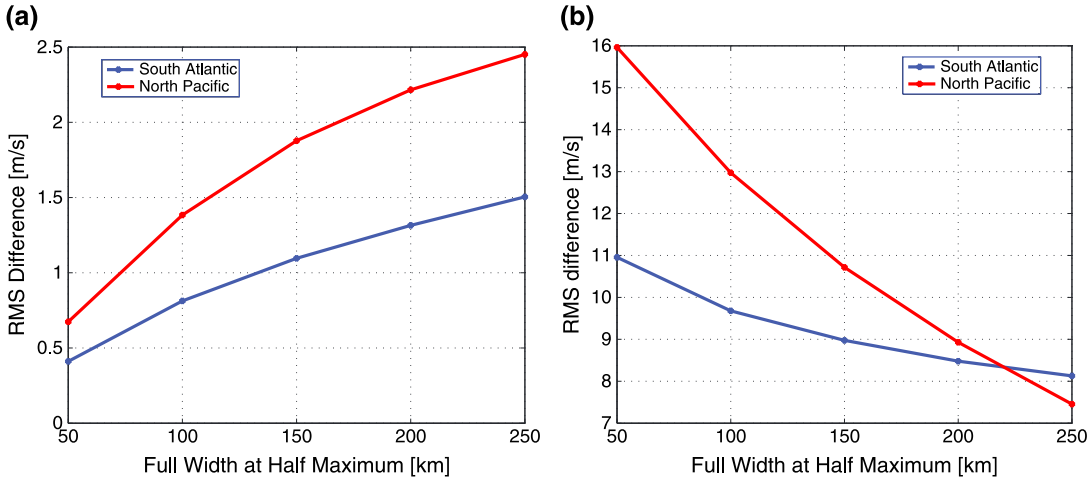

Figure 3. (a) RMS difference between original and smoothed DTU10 MSSH, as a function of FWHM. (b) RMS difference between smoothed DTU10 MSSH and TDS-1 SSH, as a function of FWHM. Note the difference in y-axis scale between the two plots.

implementing the SSH estimation algorithm. We choose an interpolation factor of 1000 and a spline interpolation method, which gives slightly lower root-mean-square (RMS) difference between TDS-1 and ground truth SSH, compared to interpolation by zero padding in the frequency domain. However, the 5 MHz bandwidth of the GPS-R receiver removes the high-frequency components of the original waveform, and they cannot be recovered by the interpolation. As stated in *Rius et al.* [2010], this band limiting is known to cause an error in the retrieved SSH.

We implement the LED algorithm on the interpolated waveforms following the approach outlined in *Hajj and Zuffada* [2003], where the first-order derivative is computed for each delay waveform and the delay value at the derivative peak represents the estimated delay difference between direct and reflected signal, denoted by τ_2 (shown in blue in Figure 2). The transmitter, receiver, and predicted specular point position contained in the DDM metadata allow for the calculation of the predicted delay difference between direct and reflected signal, denoted by τ_1.

The delay difference $\Delta\tau = (\tau_1 - \tau_2)$ is converted to SSH with knowledge of the measurement geometry, as given by

$$
\begin{aligned}
h_{\mathrm{TDS}} &= \frac{-(\alpha\beta + H_t) + \sqrt{(\alpha\beta + H_t)^2 - (\alpha^2 - 1)\cdot(\beta^2 - R_t^2)}}{\alpha^2 - 1} \\
\alpha &= \frac{H_r - H_t}{K} \\
\beta &= \frac{R_t^2 - R_r^2 + K^2}{2K} \\
K &= R_t + R_r - c\Delta\tau
\end{aligned}
\tag{1}
$$

where h_{TDS} is the estimated SSH, c is the speed of light, R_t and R_r are, respectively, the transmitter and receiver ranges from the predicted specular point on the Earth's WGS84 ellipsoid, and H_t and H_r are, respectively, the transmitter and receiver altitude with respect to the plane tangent to the WGS84 Ellipsoid at the specular point. These parameters are illustrated in Figure 2.

The estimated height h_{TDS} is susceptible to large errors due to measurement noise, orbit uncertainty, and limited receiver bandwidth. We remove the nonphysical outliers by retaining only samples that satisfy the following criterion:

$$
h_{\mathrm{TDSmean}} - 1.5(h_{\mathrm{DTUmean}} - h_{\mathrm{DTUmin}}) \le h_{\mathrm{TDS}} \le h_{\mathrm{TDSmean}} + 1.5(h_{\mathrm{DTUmax}} - h_{\mathrm{DTUmean}}) \tag{2}
$$

where h_{TDSmean} is the mean TDS-1 SSH value and h_{DTUmean}, h_{DTUmin}, and h_{DTUmax} are, respectively, the mean, minimum, and maximum DTU10 MSSH values over the region of interest. This criterion retains all estimated

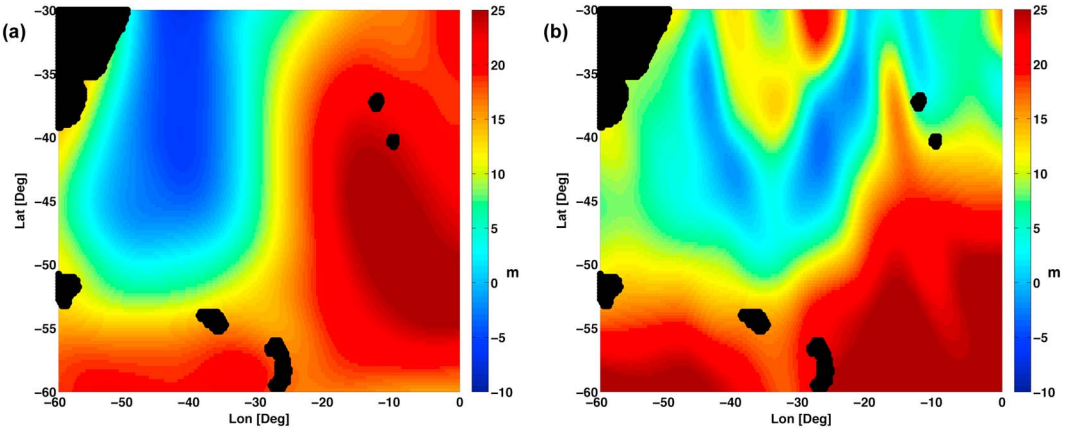

Figure 4. (a) Image of the DTU10 MSSH in South Atlantic; (b) image of TDS-1 SSH. The DTU values are subsampled at the locations of the TDS-1 samples and then the same Gaussian spatial smoothing with FWHM = 250 km is applied in both cases. An overall bias removal is also applied to the TDS-1 SSH.

SSH samples which lie within 150% of the width of the DTU10 MSSH dynamic range. It eliminates 31% of the original data for the South Atlantic region, and 14% for the North Pacific region, but in both cases it retains enough samples to perform a first-order analysis.

Individual TDS-1 estimates of SSH are sampled along isolated tracks, as shown in Figures 1b and 1c. An overall bias removal is applied to them, which forces the mean SSH estimated from TDS-1 across each region to equal the mean DTU10 SSH over the same region. This facilitates the comparison between TDS-1 and DTU10 results by emphasizing the imaging of relative SSH features. The bias that is removed is −4.3 m for the South Atlantic region and 1.7 m for the North Pacific region.

The individual samples are then spatially smoothed, and values between samples are interpolated as follows. A 0.25° latitude/longitude grid is first defined over the test regions. At each grid point, the SSH is estimated through a smoothing procedure with a Gaussian kernel of specified full width at half maximum (FWHM) [*Nixon and Aguado*, 2002]. To make the ground truth SSH (h_{DTU}) consistent, the same Gaussian smoothing is applied to the MSSH. The smoothing FWHM is chosen to be 250 km. The motivation for such choice is illustrated in Figure 3, which shows the RMS difference between original and smoothed h_{DTU} (Figure 3a) and the RMS difference between smoothed h_{DTU} and smoothed h_{TDS} (Figure 3b) as a function of FWHM. Figure 3a demonstrates that a 250 km FWHM produces an acceptable RMS difference of ~1.5–2.5 m between original and smoothed MSSH in both cases, which is small compared to the DTU MSSH dynamic range shown

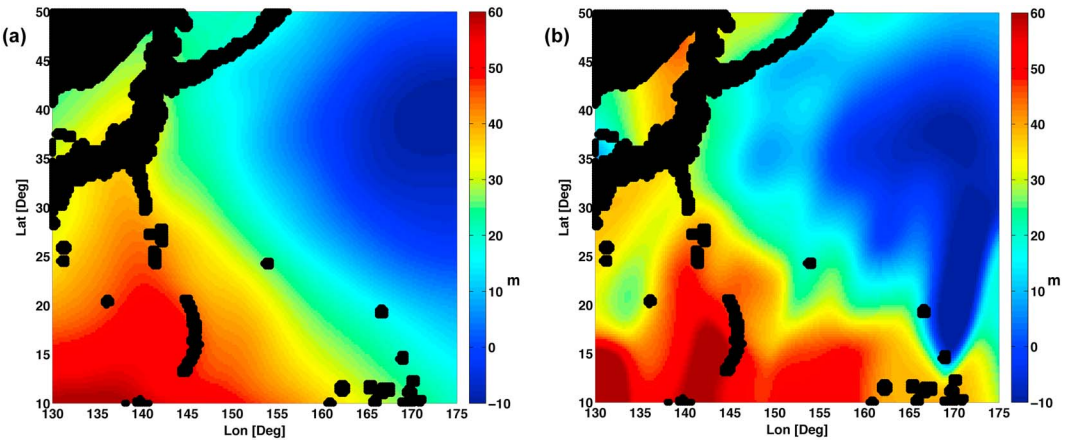

Figure 5. (a) Image of DTU10 MSSH over the North Pacific; (b) image of TDS-1 SSH. The same processing as the one described in Figure 4 is applied here.

in Figure 1, and it does not significantly change the distribution of heights in the original MSSH map. Figure 3b shows that a larger FWHM contributes to a reduction in the RMS difference between h_{TDS} and h_{DTU}.

4. Results and Discussion

Figure 4 shows the comparison between Gaussian-smoothed TDS-1 and DTU10 maps of SSH for the South Atlantic region. The GPS-R signal from TDS-1 can be seen to respond to the large-scale topography of the ocean surface, which is primarily determined by the geoid. The positive-to-negative SSH transitions are overall consistent, although in some cases they are not exactly colocated in space. Some discrepancies are observed, particularly in the northeast corner of the images, where the TDS-1 SSH values are negative but the ground truth heights are positive.

Similarly, Figure 5 shows the comparison between SSH maps for the North Pacific region. Once again, we observe an overall agreement between measured and DTU10 heights. The ringing exhibited by the TDS-1 SSH maps in both regions is the result of the differences between adjacent passes, smoothed by the gaussian filter.

The qualitative assessment of the results is promising, yet the final RMS difference between TDS-1 SSH and DTU10 MSSH is 8.1 m for the South Atlantic case and 7.4 m for the North Pacific case (Figure 3b). These differences are quite large but not surprising given that the characteristics of the GPS-R instrument onboard TDS-1 are not optimized for SSH estimation, and several large sources of error can be identified. The accuracy of the delay difference between direct and reflected signal provided in the DDM metadata is typically within one to two DDM pixel (0.25–0.50 chips). As noted in section 2, one 0.25-chip delay increment corresponds to a SSH increment of 37–50 m, and we expect a considerable SSH uncertainty even after the interpolation, since the interpolation cannot recover the high-frequency component of the waveform. An overall error calculated for simulations using the CYGNSS constellation (having similar system parameters as TDS-1), which incorporates both the error due to the limited receiver bandwidth and the error due to the noise affecting the waveforms, is estimated to be between 3.5 m and 7 m [*Zuffada et al*., 2015] depending on wind speed and geometry, for an antenna gain of 9 dBi, which represents the approximate mean antenna gain in both regions. Another significant source of error comes from the uncertainty in orbit knowledge. The receiver position calculated onboard differs from the one provided in the metadata by typically 5 m or more. This difference corresponds to a delay variation of 0.01–0.02 chips, depending on the particular geometry, which in turn translates into a SSH variation of 3 m to 5 m. The errors found in this analysis are also larger than the predicted SSH precision of ~5 m, estimated in the literature for the noninterferometric case, with simulations of spaceborne systems using the LED algorithm [see *Cardellach et al*., 2013, Table IV]. However, no orbit errors are introduced in *Cardellach et al*. [2013] since the position of the receiver is assumed known perfectly. The error in the delay estimation is considerably lower, due to the higher waveform delay resolution and higher receiver bandwidth of, respectively, 0.0125 chips and 48 MHz, as opposed to the 0.25 chips and 5 MHz for TDS-1. In addition, the TDS-1 peak antenna gain (13.3 dBi) is worse than the 19 dBi peak gain assumed in *Cardellach et al*. [2013], which contributes to an error of 1 m to 1.5 m [*Zuffada et al*., 2015]. Finally, it is important to note that the results in *Cardellach et al*. [2013] only refer to altimetric precision, whereas our errors also include residuals of the standard altimetry corrections (i.e., ionospheric, tropospheric, inverse barometer effects, sea state bias, etc.) and solid and ocean tides, after the correction for an overall bias has been applied over each entire region. Indeed, the spatial variability of these corrections over the extent of the considered regions is in any case on the order of centimeters [*Martin-Neira et al*., 2011], i.e., 1–2 orders of magnitude lower than the error caused by the orbit uncertainty, the limited receiver bandwidth, and the noise affecting the waveforms. These are three greatest sources of error in this analysis.

An improved data set is expected with the upcoming CYGNSS mission, since the information about the orbits and their accuracy will be better determined, and the DDMs will be acquired with a slightly higher antenna gain (14.5 dBi) and lower noise figure than TDS-1. However, CYGNSS will carry the same GPS-R receiver as TDS-1. Hence, the limitations related to the narrow receiver bandwidth and delay resolution of DDMs will remain.

5. Conclusions and Future Work

The ability of spaceborne GPS-Reflectometry to provide sea surface height information has been demonstrated for the first time using data from the TechDemoSat-1 satellite. SSH is derived from delay waveforms

using the LED algorithm, which locates the peak of the derivative of the return waveform along its leading edge. A QC and outlier filter are applied to the estimated SSH, followed by a spatial Gaussian smoothing with a full width at half maximum of 250 km. The same filters are applied to the DTU10 SSH, used as ground truth. The comparison between TDS-1 and DTU10 SSH is carried out for two test regions, located in the South Atlantic and North Pacific. Good agreement is observed between 2-D images of SSH, showing that GPS-R data successfully capture the large-scale variations in the surface height. The overall RMS difference is high and higher than precision estimates available in the literature, which are based on simulated spaceborne scenarios. However, the characteristics of the GPS-R instrument on board the TDS-1 satellite provide a good explanation for the errors observed, since the instrument itself is not optimized for altimetry purposes.

One important limitation of this analysis is the sparse space and time sampling of the available data, as a consequence of the GPS-R payload being switched on for only 2 out of every 8 days. However, with the launch of CYGNSS in 2016, the space-time coverage will become quite dense over ±38° latitude, allowing for a more global assessment of the SSH retrieval capabilities of spaceborne GNSS-R. Better SSH retrieval performance than TDS-1 is expected with CYGNSS due to its higher antenna gain, lower receiver noise floor, the availability of more samples, and improved orbit determination. In addition, a number of improvements to the SSH retrieval algorithm should also be considered, including the exploitation of the full DDM, the implementation of improved retracking algorithms, and the use of atmospheric and oceanographic corrections typically applied in conventional altimetry.

Acknowledgments

The authors are grateful to P. Jales at SSTL for providing additional information on the data via personal communications and to the TDS-1 Team at SSTL for the work undertaken for this mission and for making the data collected over a 6 month period publicly available, at www.merrbys.co.uk. The authors would like to thank S. Lowe and E. Cardellach for their useful discussions. Part of the research was carried out at the Jet Propulsion Laboratory, California Institute of Technology, under a contract with the National Aeronautics and Space Administration. The work presented was supported by NASA Science Mission Directorate contract NNL13AQ00C and by the JPL Innovative Spontaneous Concept R&TD Program award R.15.021.048.

References

Andersen, O. (2010), The DTU10 gravity field and mean sea surface, in *Second International Symposium of the Gravity Field of the Earth (IGFS2)*, Univ. of Alaska-Fairbanks, Fairbanks, Alaska.

Andersen, O., P. Knudsen, and P. Berry (2010), The DNSC08GRA global marine gravity field from double retracked satellite altimetry, *J. Geod.*, *84*(3), 191–199.

Camps, A., et al. (2014), Optimization and performance analysis of interferometric GNSS-R altimeters: Application to the Paris IoD mission, *IEEE J. Select. Top. Appl. Earth Obs. Remote Sens.*, *7*(5), 1436–1451, doi:10.1109/JSTARS.2014.2320873.

Cardellach, E., A. Rius, M. Martín-Neira, F. Fabra, O. Nogués-Correig, S. Ribó, J. Kainulainen, A. Camps, and S. D'Addio (2013), Consolidating the precision of interferometric GNSS-R ocean altimetry using airborne experimental data, *IEEE Trans. Geosci. Remote Sens.*, *52*(8), 4992–5004, doi:10.1109/TGRS.2013.2286257.

Clarizia, M. P., C. Ruf, P. Jales, and C. Gommenginger (2014), Spaceborne GNSS-R minimum variance wind speed estimator, *IEEE Trans. Geosci. Remote Sens.*, *52*(11), 6829–6843, doi:10.1109/TGRS.2014.2303831.

D'Addio, S., M. Martin-Neira, M. Di Bisceglie, C. Galdi, and F. Alemany (2014), GNSS-R altimeter based on doppler multi-looking, *IEEE J. Select. Top. Appl. Earth Obs. Remote Sens.*, *7*(5), 1452–1460, doi:10.1109/JSTARS.2014.2309352.

Foti, G., C. Gommenginger, P. Jales, M. Unwin, A. Shaw, C. Robertson, and J. Roselló (2015), Spaceborne GNSS-Reflectometry for ocean winds: First results from the UK TechDemoSat-1 mission, *Geophys. Res. Lett.*, *42*, 5435–5441, doi:10.1002/2015GL064204.

Garrison, J., A. Komjathy, V. Zavorotny, and S. J. Katzberg (2002), Wind speed measurements using forward scattered GPS signals, *IEEE Trans. Geosci. Remote Sens.*, *40*(1), 50–65.

Gleason, S. (2013), Space-based GNSS scatterometry: Ocean wind sensing using an empirically calibrated model, *IEEE Trans. Geosci. Remote Sens.*, *51*(9), 4853–4863, doi:10.1109/TGRS.2012.2230401.

Gleason, S., and D. Gebre-Egziabher (2009), *GNSS Applications and Methods*, pp. 399–434, Springer, Norwood, Mass.

Hajj, G. A., and C. Zuffada (2003), Theoretical description of a bistatic system for ocean altimetry using the GPS signal, *Radio Sci.*, *38*, 1089, doi:10.1029/2002RS002787.

Hall, C., and R. Cordey (1988), Multistatic scatterometry, in *Geoscience and Remote Sensing Symposium, 1988, IGARSS'88. Remote Sens.: Moving 21st Century, Int.*, vol. 1, pp. 561–562, IEEE, Edinburgh, Scotland.

Jales, P., and M. Unwin (2015a), Mission description—GNSS-Reflectometry on TDS-1 with the SGR-ReSI, *Tech. Rep. SSTL Rep. 0248367 Revision 001*, Surrey Satellite Technol. Ltd. [Available at http://www.merrbys.co.uk.]

Jales, P., and M. Unwin (2015b), MERRByS product manual: GNSS-Reflectometry on TDS-1 with the SGR-ReSI, *Tech. Rep. SSTL Rep. 0248366 Revision 001*, Surrey Satellite Technol. Ltd. [Available at http://www.merrbys.co.uk.]

Katzberg, S. J., O. Torres, and G. Ganoe (2006), Calibration of reflected GPS for tropicalstorm wind speed retrievals, *Geophys. Res. Lett.*, *33*, L18602, doi:10.1029/2006GL026825.

Lowe, S., T. Meehan, and L. Young (2014), Direct-signal enhanced semi-codeless processing of GNSS surface-reflected signals, *IEEE J. Select. Top. Appl. Earth Obs. Remote Sens.*, *7*(5), 1469–1472, doi:10.1109/JSTARS.2014.2313061.

Lowe, S. T., C. Zuffada, Y. Chao, P. Kroger, L. Young, and J. LaBrecque (2002), Five-cm-precision aircraft ocean altimetry using GPS reflections, *Geophys. Res. Lett.*, *29*(10), 1375, doi:10.1029/2002GL014759.

Martin-Neira, M. (1993), A Passive Reflectometry and Interferometry System (PARIS): Application to ocean altimetry, *ESA J.*, *17*, 331–355.

Martin-Neira, M., S. D'Addio, C. Buck, N. Floury, and R. Prieto-Cerdeira (2011), The PARIS ocean altimeter in-orbit demonstrator, *IEEE Trans. Geosci. Remote Sens.*, *49*(6), 2209–2237, doi:10.1109/TGRS.2010.2092431.

Nixon, M. S., and A. S. Aguado (2002), *Feature Extraction and Image Processing*, pp. 86–88, Elsevier, San Diego, Calif.

Pascual, D., H. Park, A. Camps, A. Alonso, and R. Onrubia (2013), Comparison of GPS L1 and Galileo E1 signals for GNSS-R ocean altimetry, in *Proceedings of International Geoscience and Remote Sensing Symposium (IGARSS)*, pp. 358–361, IEEE, Melbourne, Australia, doi:10.1109/IGARSS.2013.6721166.

Rius, A., E. Cardellach, and M. Martín-Neira (2010), Altimetric analysis of the sea-surface GPS-reflected signals, *IEEE Trans. Geosci. Remote Sens.*, *48*(4), 2119–2127, doi:10.1109/TGRS.2009.2036721.

Ruf, C., et al. (2015), New ocean winds satellite mission to probe hurricanes and tropical convection, *Bull. Am. Meteorol. Soc.*, doi:10.1175/BAMS-D-14-00218.1.

Wickert, J., et al. (2014), GEROS-ISS: Innovative ocean remote sensing using GNSS-Reflectometry onboard the international space station, in *Proceedings of the Advanced RF Sensors and Remote Sensing Instruments (ARSI) Workshop*, ESA ESTEC, Noordwijk, Netherlands.

Zuffada, C., Z. Li, S. Nghiem, S. Lowe, R. Shah, M. P. Clarizia, and E. Cardellach (2015), The rise of GNSS-Reflectometry for Earth remote sensing, in *Proceedings of the International Geoscience and Remote Sensing Symposium (IGARSS)*, IEEE, Milan, Italy.

Erratum

In the pdf of the originally published version of this article, the square root in the right-hand term of the equation was incorrectly applied to the numerator and denominator. The following errors have since been corrected in the pdf, and this version may be considered the authoritative version of record. In section 3, the square root in the right-hand term of the equation applies to the numerator only. In addition, the first addend on the right-hand side of the equation becomes part of the numerator of the second addend.